Reduced-Order Aeroelastic Models via Dynamic Residualization

M. Karpel*
Technion—Israel Institute of Technology, Haifa 32000, Israel

The accuracy of the mathematical models for aeroelastic analysis, design, and simulation is increased with the number of vibration modes chosen to represent the structure. However, the associated increase in the model size adversely affects calculation efficiency. The purpose of this work is to present a dynamic residualization method with which important structural and unsteady aerodynamic effects associated with high-frequency vibration modes are retained without increasing the model size. The formulation is based on state-space equations of motion where the unsteady aerodynamic force coefficients are represented by a minimum-state rational approximation function. The resulting model has constant coefficients and is compatible with time-domain simulation techniques and with modern control methods. The analytical development and a numerical example that employs a realistic aircraft model are presented. Comparisons of the reduced-order model errors with those obtained by mode truncation and by static residualization show that the dynamic residualization yields significantly more accurate models than those obtained by the other reduction techniques.

Nomenclature

$[A],[B],\{B_w\}$ = aeroservoelastic system matrices, Eqs. (9) and (10)
$[\tilde{A}],[\tilde{B}],\{\tilde{B}_w\}$ = reduced-order matrices, Eq. (18)
$[\bar{A}],\{\bar{B}_w\}$ = closed-loop system matrices, Eqs. (14) and (25)
$[A_c],[B_c]$ = control system matrices, Eq. (6)
$[A_g],\{B_g\}$ = gust dynamic matrix and noise distribution vector, Eq. (8)
$[A_0],[A_1],[A_2]$ = matrix coefficients of the aerodynamic approximation, Eq. (3)
$[B_s]$ = generalized structural damping matrix
b = reference semichord
$[C_{c_0}],[C_{c_1}],[C_{c_2}]$ = partitions of the control system output matrix, Eq. (6)
$[C_{g_0}],[C_{g_1}],\{D_{g_1}\}$ = gust output matrices, Eq. (8)
$[C],\{D_w\}$ = output matrices, defined in Eqs. (11) and (12)
$[\tilde{C}],[\tilde{D}],\{\tilde{D}_w\}$ = reduced-order matrices, Eq. (18)
$[\bar{D}]$ = defined in Eq. (5)
$[D],[E]$ = approximation coefficient matrices, Eq. (3)
$[F_1],[F_2]$ = defined in Eqs. (19) and (23)
$[F],[G],\{G_w\},[H]$ = constraint matrices of Eq. (16), defined in Eq. (20) or (24)
$[\bar{F}_c],[\bar{F}_g],\{\bar{F}_w\}$ = force coefficients matrices, Eq. (10)
$[G_c]$ = control gain matrix, Eq. (13)
$[I]$ = unit matrix
$[K_s]$ = generalized stiffness matrix
$[\bar{K}_c],[\bar{K}_g],[\bar{K}_s]$ = defined in Eq. (5)
k = reduced frequency, $=\omega b/V$
k_f,k_g = k values at which data-match constraints are applied, Eqs. (27) and (28)
$[M_c],[M_s]$ = control and structure related partitions of the generalized mass matrix
$[\bar{M}_c],[\bar{M}_s]$ = defined in Eq. (5)
n = total number of model states
$[Q],[\tilde{Q}]$ = tabulated and approximated complex generalized aerodynamic matrices
$[Q_c],[Q_g],[Q_s]$ = control, gust, and structure related partitions of $[Q]$
q = dynamic pressure
$[R]$ = aerodynamic lag matrix, Eq. (3)
$[\bar{R}]$ = defined in Eq. (5)
s = Laplace variable
$\bar{s}$ = nondimensionalized Laplace variable, $=sb/V$
$\{u\}$ = control input vector
V = true air speed
w = process noise parameter
$\{w_g\}$ = gust velocity vector
$\{x\}$ = state vector
$\{x_a\},\{x_c\},\{x_g\}$ = aerodynamic, control, and gust state vectors
$\{y\}$ = sensor output vector
$[Z]$ = expanded mass matrix, Eqs. (9) and (10)
$[\tilde{Z}]$ = defined in Eq. (18)
$\{\delta\}$ = control surface rotation vector
$\{\xi\}$ = generalized structural displacements vector
$[\phi],[\phi']$ = modal displacement and slope matrices
ω = vibration frequency

Subscripts

ac = acceleration related
av = angular velocity related
c = related to the control modes
e = related to the eliminated states
g = related to the gust modes
r = related to the retained states
s = related to the structural modes
w = process noise related

Received March 4, 1989; revision received Oct. 20, 1989.

*Senior Research Associate, Faculty of Aerospace Engineering. Member AIAA.

Introduction

THE common approach for formulating the equations of motion of an aeroelastic system[1,2] starts with a normal modes analysis of the structural system. A realistic, continuous structural system has an infinite number of vibration modes. However, many flutter, structural dynamic response, and aircraft performance issues may be adequately analyzed with a limited set of low frequency vibration modes (including rigid-body modes). Control surface deflection modes are added to account for the interaction between the aeroelastic and control systems with an aeroservoelastic model. Gust velocity modes may also be added to analyze the response of the structural and control systems to continuous gust.

The structural, control surface, and gust modes serve as generalized coordinates with respect to which unsteady aerodynamic force coefficients are defined. The most commonly used unsteady aerodynamic routines, such as those based on the doublet lattice method (DLM)[3], assume that the structure oscillates harmonically. Transcendental unsteady aerodynamic matrices are calculated for various reduced frequency values. Second-order, frequency-domain formulations can be used for iterative stability solutions,[4] frequency response, and frequency-domain control synthesis. However, application of various modern control design techniques,[5,6] integrated simulations,[7] and optimization[8] procedures requires the equations of motion to be cast in a first-order, time-domain (state-space) form. This formulation is based on a rational approximation of the transcendental aerodynamic matrices. The number of denominator roots of the approximation function define the number of augmented aerodynamic states. Tiffany and Adams[9] reviewed and extended various approximation methods, and applied them in NASA's Interaction of Structures, Aerodynamics and Controls (ISAC) Computer program.[10] Among those, the minimum-state method of Karpel[11,12] yields the lowest number of aerodynamic states per required accuracy. Various applications of the minimum-state methods[12-14] show that the number of aerodynamic states required to obtain good accuracy is about one-fifth of the number of structural states. The augmentation of control system and gust related state (as in Ref. 6) completes the state-space aeroservoelastic model.

A key question that the analyst faces is how many structural modes should be taken into account. The analysis may start with a relatively large number of modes with which the basic aeroservoelastic behavior is studied and the frequency range of interest (the range in which there is a considerable aeroelastic activity) is defined. However, efficient subsequent applications such as control system design, time simulation, parametric studies, and structural and/or control system optimization may require the model to be as small as possible but with acceptable accuracy.

A simple truncation of vibration modes with natural frequencies above the range of interest reduces the model size but might yield unacceptable errors. A way to take into account steady effects of the eliminated modes without increasing the model size is by a static residualization such as that of Sheena and Karpel.[15] This process, which yields accurate results in analyzing the "rigid-body" dynamics, may not be accurate enough in higher frequency flutter mechanisms. The purpose of this work is to develop a dynamic residualization method in which unsteady effects of the eliminated modes are added to those of the static residualization without increasing the model size. Application to a realistic aeroservoelastic model will demonstrate the costs and benefits of low-order aeroelastic modeling via dynamic residualization.

Full-Size Model

The equations of motion in this paper follow the time-domain aeroservoelastic modeling technique of Ref. 12. The Laplace transform of the open-loop aeroelastic system equation of motion, excited by control surface motions and gust velocities reads

$$\Big([M_s]s^2+[B_s]s+[K_s]+q[Q_s(s)]\Big)\Big\{\xi(s)\Big\} = -\Big([M_c]s^2+q[Q_c(s)]\Big)\Big\{\delta(s)\Big\} - \frac{q}{V}[Q_g(s)]\Big\{w_g(s)\Big\} \quad (1)$$

In order to transform Eq. (1) into a time-domain constant coefficient equation, the aerodynamic matrices have to be described as rational functions of s. The minimum-state method[11,12] approximates $[Q(s)]$ by

$$[\bar{Q}(\bar{s})] = [A_0] + [A_1]\bar{s} + [A_2]\bar{s}^2 + [D]\Big(\bar{s}[I]-[R]\Big)^{-1}[E]\bar{s} \quad (2)$$

where $[R]$ is a diagonal matrix with distinct negative terms representing the aerodynamic lags. The real-valued approximation matrices of Eq. (2) are partitioned into structural-, control-, and gust-mode related terms as

$$[A_i] = \begin{bmatrix} A_{s_i} & A_{c_i} & A_{g_i} \end{bmatrix} \qquad \text{for } i = 0,1,2$$

$$[D] = [D_s] \qquad [E] = [E_s \quad E_c \quad E_g] \quad (3)$$

The approximation procedure converges for the coefficient matrices that best fit a set of $[Q(ik)]$ matrices, tabulated for various reduced-frequency (k) values.

The resulting time-domain, open-loop plant equation of motion, with the constraint of $[A_{g_2}]=0$ (to avoid an unnecessary $\ddot{w}_g$ term) is

$$\begin{bmatrix} I & 0 & 0 \\ 0 & \bar{M}_s & 0 \\ 0 & 0 & I \end{bmatrix}\begin{Bmatrix} \dot{\xi} \\ \ddot{\xi} \\ \dot{x}_a \end{Bmatrix} = \begin{bmatrix} 0 & I & 0 \\ -\bar{K}_s & -\bar{B}_s & -\bar{D} \\ 0 & E_s & \bar{R} \end{bmatrix}\begin{Bmatrix} \xi \\ \dot{\xi} \\ x_a \end{Bmatrix} + \begin{bmatrix} 0 & 0 & 0 \\ -\bar{K}_c & -\bar{B}_c & -\bar{M}_c \\ 0 & E_c & 0 \end{bmatrix}\begin{Bmatrix} \delta \\ \dot{\delta} \\ \ddot{\delta} \end{Bmatrix} + \begin{bmatrix} 0 & 0 \\ -\bar{K}_g & -\bar{B}_g \\ 0 & E_g \end{bmatrix}\begin{Bmatrix} w_g \\ \dot{w}_g \end{Bmatrix} \quad (4)$$

where

$$[\bar{M}_s] = [M_s] + \frac{qb^2}{V^2}[A_{s_2}], \qquad [\bar{K}_s] = [K_s] + q[A_{s_0}]$$

$$[\bar{B}_s] = [B_s] + \frac{qb}{V}[A_{s_1}], \qquad [\bar{K}_c] = q[A_{c_0}]$$

$$[\bar{B}_c] = \frac{qb}{V}[A_{c_1}], \qquad [\bar{M}_c] = [M_c] + \frac{qb^2}{V^2}[A_{c_2}]$$

$$[\bar{K}_g] = q[A_{g_0}], \qquad [\bar{B}_g] = \frac{qb}{V}[A_{g_1}]$$

$$[\bar{D}] = q[D], \qquad [\bar{R}] = \frac{V}{b}[R] \quad (5)$$

A linear transfer function of the control system (including the actuators) can be described in a state-space form as

$$\{\dot{x}_c\} = [A_c]\{x_c\} + [B_c]\{u\}$$

$$\begin{Bmatrix} \delta \\ \dot{\delta} \\ \ddot{\delta} \end{Bmatrix} = \begin{bmatrix} C_{c_0} \\ C_{c_1} \\ C_{c_2} \end{bmatrix} \{x_c\} \tag{6}$$

The aeroservoelastic loop is closed by relating the control input vector $\{u\}$ to the output of angular velocity meters $\{y_{av}\}$ and accelerometers $\{y_{ac}\}$. The sensor dynamics are neglected in this work, which yields

$$\{y_{av}\} = [\phi']\{\dot{\xi}\}, \qquad \{y_{ac}\} = [\phi]\{\ddot{\xi}\} \tag{7}$$

where $[\phi]$ and $[\phi']$ are the modal displacements and modal slopes at the sensor input.

The gust velocities are defined in statistical terms by their power spectral density (PSD) functions. An equivalent gust dynamic system (see Ref. 6) can be defined by

$$\{\dot{x}_g\} = [A_g]\{x_g\} + \{B_g\}w$$

$$\begin{Bmatrix} w_g \\ \dot{w}_g \end{Bmatrix} = \begin{bmatrix} C_{g_0} \\ C_{g_1} \end{bmatrix} \{x_g\} + \begin{Bmatrix} 0 \\ D_{g_1} \end{Bmatrix} w \tag{8}$$

such that w represents a white-noise process with a constant PSD of unit magnitude, which has algebraic advantages in a continuous gust response analysis and fits optimal control algorithms well.

Equations (4) and (6-8) combine for the state-space aeroservoelastic model

$$[Z]\{\dot{x}\} = [A]\{x\} + [B]\{u\} + \{B_w\}w$$

$$\{y\} = [C]\{x\} + \{D_w\}w \tag{9}$$

where the system matrices are

$$\{x\} = \begin{Bmatrix} \xi \\ \dot{\xi} \\ x_a \\ x_c \\ x_g \end{Bmatrix} \qquad [Z] = \begin{bmatrix} I & & & & 0 \\ & \bar{M}_s & & & \\ & & I & & \\ & & & I & \\ 0 & & & & I \end{bmatrix}$$

$$[A] = \begin{bmatrix} 0 & I & 0 & 0 & 0 \\ -\bar{K}_s & -\bar{B}_s & -\bar{D} & -\bar{F}_c & -\bar{F}_g \\ 0 & E_s & \bar{R} & E_c & E_g \\ 0 & 0 & 0 & A_c & 0 \\ 0 & 0 & 0 & 0 & A_g \end{bmatrix}$$

$$[B] = \begin{bmatrix} 0 \\ 0 \\ 0 \\ B_c \\ 0 \end{bmatrix}, \qquad \{B_w\} = \begin{Bmatrix} 0 \\ -\bar{F}_w \\ 0 \\ 0 \\ B_g \end{Bmatrix} \tag{10}$$

where

$$[\bar{F}_c] = [\bar{K}_c][C_{c_0}] + [\bar{B}_c][C_{c_1}] + [\bar{M}_c][C_{c_2}]$$

$$[\bar{F}_g] = [\bar{K}_g][C_{g_0}] + [\bar{B}_g][C_{g_1}] \qquad \{\bar{F}_w\} = [\bar{B}_g]\{D_{g_1}\}$$

The output matrices of Eq. (9) for the angular velocity measurements of Eq. (7) are

$$[C] = [0 \quad \phi' \quad 0 \quad 0 \quad 0] \qquad \{D_w\} = \{0\} \tag{11}$$

and for the acceleration measurements of Eq. (7), using Eq. (10),

$$[C] = -[\phi][\bar{M}_s]^{-1}[\bar{K}_s \quad \bar{B}_s \quad \bar{D} \quad \bar{F}_c \quad \bar{F}_g]$$

$$\{D_w\} = -[\phi][\bar{M}_s]^{-1}\{\bar{F}_w\} \tag{12}$$

The aeroservoelastic loop is closed by relating the control input to the system output,

$$\{u\} = [G_c]\{y\} \tag{13}$$

The substitution of Eq. (13) into Eq. (9) yields the closed-loop equation of motion

$$[Z]\{\dot{x}\} = [\bar{A}]\{x\} + \{\bar{B}_w\}w \tag{14}$$

where

$$[\bar{A}] = [A] + [B][G_c][C] \qquad \{\bar{B}_w\} = \{B_w\} + [B][G_c]\{D_w\}$$

It may be noticed from $[B]$ of Eq. (10) that only the fourth row partitions of $[\bar{A}]$ and $\{\bar{B}_w\}$ are different than those of $[A]$ and $\{B_w\}$.

Model Size Reduction

General

It is assumed that a full-size model (with the initial set of vibration modes) has been established and that the analyst has defined a frequency range of important aeroelastic activity. The state vector $\{x\}$ is partitioned into subsets $\{x_r\}$ and $\{x_e\}$ where $\{x_e\}$ is to be constrained and eliminated from the independent state vector. In our case, $\{x_e\}$ includes the states $\{\xi_e\}$ and $\{\dot{\xi}_e\}$, which represent the vibration modes with natural frequencies beyond the frequency range of interest. It is assumed that some of the dynamics associated with $\{x_e\}$ have negligible effects on the aeroelastic behavior of $\{x_r\}$.

The partitioning of Eq. (9) into $\{x_r\}$ and $\{x_e\}$ related partitions yields

$$\begin{bmatrix} Z_{rr} & Z_{re} \\ Z_{er} & Z_{ee} \end{bmatrix} \begin{Bmatrix} \dot{x}_r \\ \dot{x}_e \end{Bmatrix} = \begin{bmatrix} A_{rr} & A_{re} \\ A_{er} & A_{ee} \end{bmatrix} \begin{Bmatrix} x_r \\ x_e \end{Bmatrix} + \begin{bmatrix} B_r \\ B_e \end{bmatrix} \{u\} + \begin{Bmatrix} B_{w_r} \\ B_{w_e} \end{Bmatrix} w$$

$$\{y\} = [C_r \quad C_e] \begin{Bmatrix} x_r \\ x_e \end{Bmatrix} + \{D_w\}w \tag{15}$$

where $[B_e] = 0$ because $\{x_e\}$ is based on vibration modes only. With the assumption that the $\{\dot{x}_e\}$ effects on the top partition of Eq. (15) (through $[Z_{re}]$) may be neglected, the most general constraints that allow model size reduction are

$$\{x_e\} = [F]\{x_r\} + [G]\{u\} + \{G_w\}w + [H]\{\dot{x}_r\} \tag{16}$$

where the last term of Eq. (16) is introduced for convenience in the following formulation, which defines the coefficient matrices $[F]$, $[G]$, $\{G_w\}$, and $[H]$ according to the size reduction method. The substitution of Eq. (16) into the top partition

of Eq. (15) with $[Z_{re}]\{\dot{x}_e\}=0$ yields

$$[\tilde{Z}]\{\dot{x}_r\} = [\tilde{A}]\{x_r\} + [\tilde{B}]\{u\} + \{\tilde{B}_w\}w$$
$$\{y\} = [\tilde{C}]\{x_r\} + [\tilde{D}]\{u\} + \{\tilde{D}_w\}w \qquad (17)$$

where the matrix coefficients are

$$[\tilde{Z}] = [Z_{rr}] - [A_{re}][H]$$
$$[\tilde{A}] = [A_{rr}] + [A_{re}][F]$$
$$[\tilde{B}] = [B_r] + [A_{re}][G]$$
$$\{\tilde{B}_w\} = \{B_{w_r}\} + [A_{re}]\{G_w\}$$
$$[\tilde{C}] = [C_r] + [C_e]\left([F] + [H][\tilde{Z}]^{-1}[\tilde{A}]\right)$$
$$[\tilde{D}] = [C_e]\left([G] + [H][\tilde{Z}]^{-1}[\tilde{B}]\right)$$
$$\{\tilde{D}_w\} = \{D_w\} + [C_e]\left(\{G_w\} + [H][\tilde{Z}]^{-1}\{\tilde{B}_w\}\right) \qquad (18)$$

Mode Truncation

The simplest and most commonly used constraint assumption is that the high-frequency modes have negligible effects on the retained model, namely the constraint matrices $[F]$, $[G]$, $\{G_w\}$, and $[H]$ of Eq. (16) are all zero. The resulting model is that of Eq. (15) where all of the rows and columns associated with $\{x_e\}$ are truncated.

Static Residualization

The static residualization is based on the principles of static aeroelastic analysis using vibration modes (such as in Ref. 15) where the aerodynamics associated with the deflections of the elastic modes have a major impact on the rigid-body aerodynamics. In the present case, it is assumed that the $\{\xi_e\}$ effects are important but the $\{\dot{\xi}_e\}$ and $\{\ddot{\xi}_e\}$ effects may be neglected (as done in ISAC[10]). With these assumptions, the bottom row partition of the equation of motion [Eq. (15)] and the matrix definitions of Eq. (10) yield

$$[\bar{K}_{s_{ee}}]\{\xi_e\} = [F_1]\{x_r\} - \{\bar{F}_{w_e}\}w - [\bar{M}_{s_{er}}]\{\ddot{\xi}_r\} \qquad (19)$$

where

$$[F_1] = \left[-\bar{K}_{s_{er}} \quad -\bar{B}_{s_{er}} \quad -\bar{D}_e \quad -\bar{F}_{c_e} \quad -\bar{F}_{g_e}\right]$$

Equation (19) and $\{\dot{\xi}_e\}=\{0\}$ yield the constraint matrices of Eq. (16) for the case of static residualization

$$[F] = \begin{bmatrix}\bar{K}_{s_{ee}}^{-1}\\ 0\end{bmatrix}[F_1], \quad [G] = [0], \quad \{G_W\} = -\begin{bmatrix}\bar{K}_{s_{ee}}^{-1}\\ 0\end{bmatrix}\{\bar{F}_{w_e}\}$$
$$[H] = -\begin{bmatrix}\bar{K}_{s_{ee}}^{-1}\\ 0\end{bmatrix}\begin{bmatrix}0 & \bar{M}_{s_{er}} & 0 & 0 & 0\end{bmatrix} \qquad (20)$$

The statically residualized reduced-order model of Eq. (17) can now be constructed using Eq. (18). It can be shown from Eqs. (10), (18), and (20) that $[\tilde{Z}]$, $[\tilde{A}]$, and $\{\tilde{B}_w\}$ have the same topology (nonzero partitions) as $[Z_{rr}]$, $[A_{rr}]$, and $\{B_{w_r}\}$, that $[\tilde{B}]=[B_r]$, and that $[\tilde{D}]=[0]$. The closed-loop equation of motion can be constructed by Eq. (14) where $[A]$, $[B]$, $[C]$, $\{B_w\}$, and $\{D_w\}$ are replaced by those of Eq. (18). It should be noted that the assumption of $\{\ddot{\xi}_e\}=0$ in Eq. (20) does not mean that the eliminated modes do not move. It only means that the forces associated with this motion are neglected.

Dynamic Residualization

The dynamic residualization suggested in this work does not neglect a priori the aerodynamic effects of $\{\dot{\xi}_e\}$. The extension of Eq. (19) to include these effects reads

$$[\bar{K}_{s_{ee}}]\{\xi_e\} = [F_1]\{x_r\} - \{\bar{F}_{w_e}\}w - [\bar{M}_{s_{er}}]\{\ddot{\xi}_r\} - [\bar{B}_{s_{ee}}]\{\dot{\xi}_e\} \qquad (21)$$

where the first term on the right side is the primary contributor to the generalized forces acting on the eliminated modes and the other terms have secondary effects. The differentiation of Eq. (21) with respect to time, while neglecting the derivatives of the secondary effects and using the definition of $[F_1]$ in Eq. (19), yields an equation for $\{\dot{\xi}_e\}$:

$$[\bar{K}_{s_{ee}}]\{\dot{\xi}_e\} = -[\bar{K}_{s_{er}}]\{\dot{\xi}_r\} - [\bar{B}_{s_{er}}]\{\ddot{\xi}_r\} - [\bar{D}_e]\{\dot{x}_a\} - [\bar{F}_{c_e}]\{\dot{x}_c\} - [\bar{F}_{g_e}]\{\dot{x}_g\} \qquad (22)$$

which, by using Eq. (9) for $\{\dot{x}_a\}$, $\{\dot{x}_c\}$, and $\{\dot{x}_g\}$, becomes

$$[X_{22}]\{\dot{\xi}_e\} = [F_2]\{x_r\} - [\bar{F}_{c_e}][B_c]\{u\} - [\bar{F}_{g_e}]\{B_g\}w - [\bar{B}_{s_{er}}]\{\ddot{\xi}_r\} \qquad (23)$$

where

$$[X_{22}] = [\bar{K}_{s_{ee}}] + [\bar{D}_e][E_{s_e}]$$
$$[F_2] = \left[0 - (\bar{K}_{s_{er}} + \bar{D}_e E_{s_r}) - \bar{D}_e\bar{R} - (\bar{D}_e E_c + \bar{F}_{c_e}A_c) - (\bar{D}_e E_g + \bar{F}_{g_e}A_g)\right]$$

Equations (21) and (23) combine the constraint equation [Eq. (16)] with the matrix coefficients for the case of dynamic residualization:

$$[F] = [X]^{-1}\begin{bmatrix}F_1\\ F_2\end{bmatrix}, \quad [G] = -[X]^{-1}\begin{bmatrix}0\\ \bar{F}_{c_e}B_c\end{bmatrix}$$
$$\{G_w\} = -[X]^{-1}\begin{Bmatrix}\bar{F}_{w_e}\\ \bar{F}_{g_e}B_g\end{Bmatrix}$$
$$[H] = -[X]^{-1}\begin{bmatrix}0 & \bar{M}_{s_{er}} & 0 & 0 & 0\\ & \bar{B}_{s_{er}} & & & \end{bmatrix} \qquad (24)$$

where

$$[X]^{-1} = \begin{bmatrix}\bar{K}_{s_{ee}}^{-1} & -\bar{K}_{s_{ee}}^{-1}\bar{B}_{s_{ee}}X_{22}^{-1}\\ 0 & X_{22}^{-1}\end{bmatrix}$$

The dynamically residualized reduced-order model [Eq. (17)] can now be constructed by Eq. (18) with the matrices of Eq. (24). It can be shown from Eqs. (10), (18), and (24) that $[\tilde{Z}]$ still has the same topology as $[Z_{rr}]$. However, unlike the static residualization, the topology of $[\tilde{A}]$, $[\tilde{B}]$, and $\{\tilde{B}_w\}$ resulting from the dynamic residualization does not keep the original topology of $[A]$, $[B]$, and $\{B_w\}$. In addition, $[\tilde{D}]\neq 0$, which

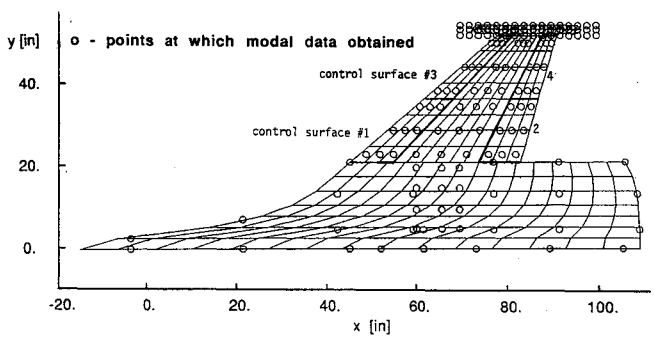

Fig. 1 AFW aerodynamic model.

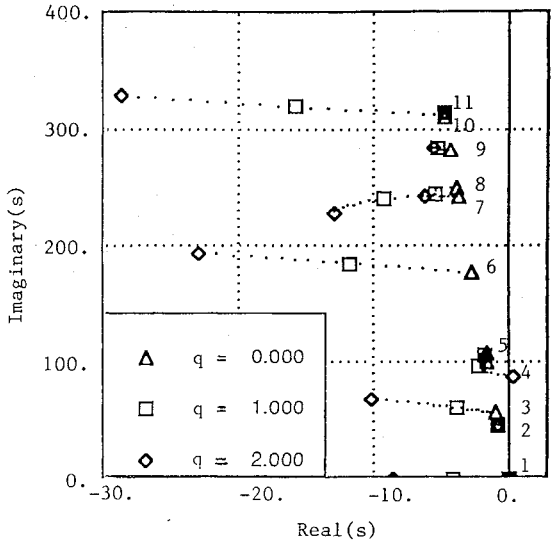

Fig. 2 Full-size, open-loop root loci.

yields the closed-loop equation of motion

$$[\tilde{Z}]\{\dot{x}_r\} = [\tilde{A}]\{x_r\} + \{\tilde{B}_w\}w \tag{25}$$

where

$$[\tilde{A}] = [\tilde{A}] + [\tilde{B}][G_c]\Big([I] - [\tilde{D}][G_c]\Big)^{-1}[\tilde{C}]$$

$$\{\tilde{B}_w\} = \{\tilde{B}_w\} + [\tilde{B}][G_c]\Big([I] - [\tilde{D}][G_c]\Big)^{-1}\{\tilde{D}_w\}$$

Aerodynamic Approximation Constraints

The minimum-state aerodynamic approximation procedure,[12,13] which results in the approximation coefficient matrices of Eqs. (2) and (3), is based on a nonlinear, least-square fit of tabulated complex aerodynamic matrices. These input matrices, $[Q(ik_\ell)]$, are given for various values of k_ℓ. The approximation procedure requires each term of $[Q]$ to be assigned with three approximation constraints. The constraints are

$$[A_0] = \mathrm{Re}[Q(0)] \tag{26}$$

either

$$\mathrm{Im}[\tilde{Q}(ik_g)] = \mathrm{Im}[Q(ik_g)] \quad \text{at a} \quad k_g \neq 0 \tag{27}$$

or

$$[A_1] = [0]$$

either

$$\mathrm{Re}[\tilde{Q}(ik_f)] = \mathrm{Re}[Q(ik_f)] \quad \text{at a} \quad k_f \neq 0 \tag{28}$$

or

$$[A_2 = [0]$$

Each term of $[Q]$ may be assigned with a different set of constraints, and the analyst is free to choose between the data-match and the zero coefficient options in Eqs. (27) and (28). The data-match options typically yield a better fit.[13] However, since the $[A_{s_1}]_{ee}$, $[A_{g_1}]_e$, $[A_{s_2}]_{re}$, $[A_{s_2}]_{er}$, and $[A_{s_2}]_{ee}$ partitions of Eq. (3) are neglected in the development of Eq. (22), constraining them to be zero may yield a better accuracy in the subsequent residualization process.

Numerical Example

Full-Size Model

The numerical application deals with Rockwell's active flexible wing (AFW) wind-tunnel model to be tested at the Transonic Dynamics Tunnel, NASA Langley Research Center. A top view of the aerodynamic model is given in Fig. 1. The circles indicate points at which modal data were obtained from the vibration analysis. The full-size mathematical model consists of 11 antisymmetric vibration modes (1 rigid-body roll and 10 elastic modes), and 4 control-surface deflection modes. The minimum-state method is used to approximate the Mach 0.9 doublet lattice, tabulated, generalized, unsteady aero-dynamic matrices with four approximation roots, which yields four aerodynamic augmented states. The 10 tabulated aerodynamic matrices are with reduced frequencies between $k = 0$ and 0.6. The "regular" data-match constraint options of Eqs. (27) and (28) with $k_f = k_g = 0.6$ are first used for all the aerodynamic terms. Four third-order irreversible actuators are used to drive the control surfaces. The constant gain (zero-order) control system reads a single roll-rate measurement and commands each actuator according to its assigned control gain. The total order of the closed-loop system is 38 (22 structural, 4 aerodynamic, and 12 actuator states).

The intended use of the aeroservoelastic model is for designing a control system that would yield adequate aircraft roll performance without violating the required flutter, gain, and phase margins. The open-loop root loci with varying dynamic pressure (q) are shown in Fig. 2. Interpolation of the branch that crosses the imaginary axis yields the flutter dynamic pressure $q_f = 1.9217$ psi and flutter frequency $\omega_f = 87.698$ rad/s. A preliminary closed-loop analysis has indicated that the control system may have a considerable effect on the aeroelastic be-

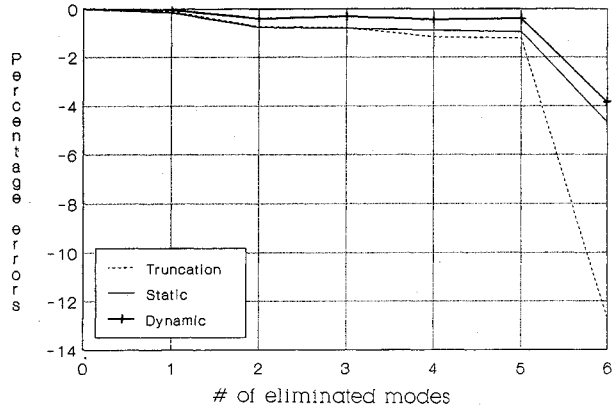

Fig. 3 Flutter dynamic pressure errors, open-loop, regular constraints.

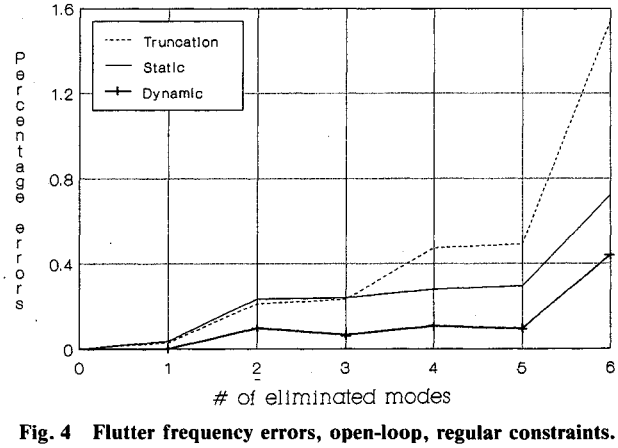

Fig. 4 Flutter frequency errors, open-loop, regular constraints.

havior in the frequency range of 0–150 rad/s. The purpose of our example is to reduce the model size by eliminating the high-frequency-related structural states in order to facilitate an efficient subsequent control design process (which is by itself beyond the scope of this work).

Model-Size Reduction

The reduced-order model of Eq. (17) has been established by mode truncation, static residualization [Eq. (18) via Eq. (20)], and dynamic residualization [Eq. (18) via Eq. (24)]. The reductions were repeated for $i = 1$–6 where i is the number of highest frequency eliminated modes. Open-loop root-loci analyses were performed with the reduced-order models. The resulting flutter dynamic presure and flutter frequency percentage errors (relative to those of the full-size model) are given in Figs. 3 and 4. It may be observed that the five highest frequency modes (modes 7–11) have a small effect on the flutter mechanism relative to that of mode 6.

A sample closed-loop root-locus analysis has been performed with $[G_c]^T = [0, -0.124, 0.1, 0.05]$. The resulting full-size flutter dynamic pressure and flutter frequency are $q_f = 1.783$ psi and $\omega_f = 88.036$ rad/s. The reduced-order flutter dynamic pressure and flutter-frequency percentage errors are given in Table 1. Here again, modes 7–11 have a small effect on the flutter mechanism, whereas the effect of mode 6 is even larger than that in the open-loop analysis. It may be concluded that mode 6 should not be eliminated as its dynamics (namely the effects of its acceleration) are not negligible. This demonstrates that reducing the order of the aeroelastic equations should be done judiciously so that the essential flutter mechanisms are kept. It can also be observed from Figs. 3 and 4 and from Table 1 that residualization yields significantly better

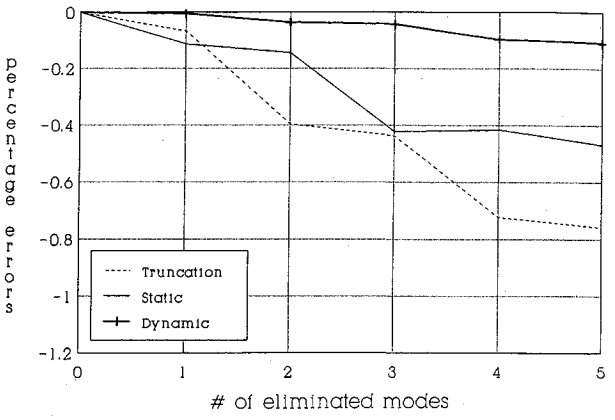

Fig. 5 Flutter dynamic pressure errors, open-loop, special constraints.

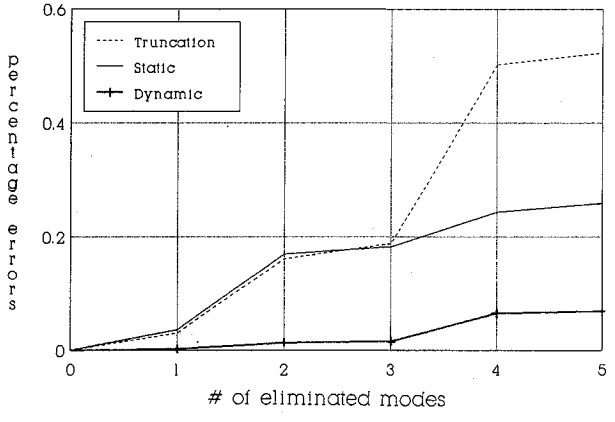

Fig. 6 Flutter frequency errors, open-loop, special constraints.

Table 1 Closed-loop flutter dynamic pressure and frequency percentage errors in reduced-order models

Number of eliminated modes	Mode truncation error, %		Static res. error, %		Dynamic res. error, %	
	q_f	ω_f	q_f	ω_f	q_f	ω_f
1	−0.056	0.035	−0.185	0.052	−0.002	0.001
2	−0.561	0.092	−0.791	0.111	−0.449	0.098
3	−1.206	0.203	−0.869	0.109	−0.280	0.068
4	−1.178	0.448	−0.841	0.153	−0.561	0.118
5	−1.122	0.465	−0.897	0.177	−0.505	0.107
6	−19.686	2.831	−6.579	1.002	−6.188	0.892

Table 2 Comparison of full-size flutter parameters resulting from different aerodynamic approximation constraints

Aerodynamic approximation constraints	Open loop		Closed loop	
	q_f, psi	ω_f, rad/s	q_f, psi	ω_f, rad/s
Regular	1.9217	87.6984	1.7830	88.0361
Special	1.9245	87.6619	1.7893	87.9554
Difference, %	0.146	−0.042	0.353	−0.092

Table 3 Root extraction time of various full-size and reduced-order models

		Full-size model	Truncated	Statically residualized	Dynamically residualized
Open loop	n	26	16	16	16
	t, s	0.54	0.12	0.15	0.18
Closed loop	n	38	28	28	28
	t, s	1.60	0.58	0.63	0.69

results than truncation and that the dynamic residualization errors are about one-half of those of the static one.

Effects of Approximation Constraints

The aerodynamics approximation has been reestablished with the coefficient constraints of $[A_{s_1}]_{ee} = [A_{s_2}]_{re} = [A_{s_2}]_{er} = [0]$ where subscript e refers to the five highest frequency eliminated modes. The other aerodynamic coefficients have the same data-match constraints as in the previous subsections. The full-size open- and closed-loop flutter dynamic pressure and frequency resulting from these "special" constraints are compared in Table 2 to those of the "regular" constraints. Because the data-match constraints usually yield a better aerodynamic approximation than the special coefficient constraints (Ref. 13), the differences presented in Table 2 may be considered as the errors introduced by the special constraints.

The flutter dynamic pressure and frequency errors due to model size reductions of the special constraint cases are shown in Figs. 5–8. Comparisons with Figs. 3 and 4 and Table 1 show that the truncation and static residualization errors in the special constraint cases are similar to those of the regular constraints, whereas the dynamic residualization errors are reduced to about one-half of those with the regular constraints. However, since the aerodynamic approximation accuracy loses (see Table 2) are similar to the residualization accuracy gains, the application of the special coefficient constraints is not worthwhile in this example.

Computation Time

The main motivation for reducing the model size is to save computation time. A basic task, which is repeated numerous times in various analyses, is the calculation of the system roots

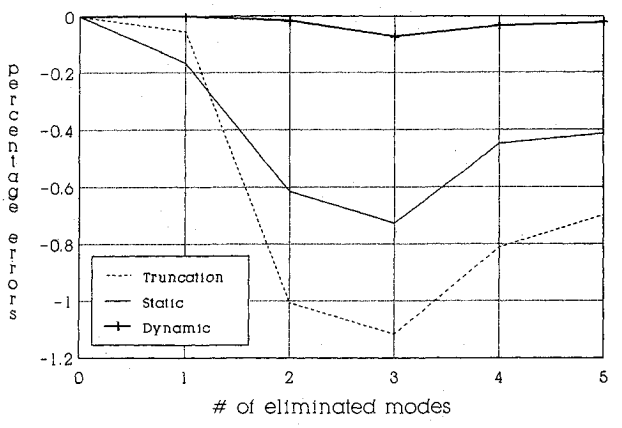

Fig. 7 Flutter dynamic pressure errors, closed-loop, special constraints.

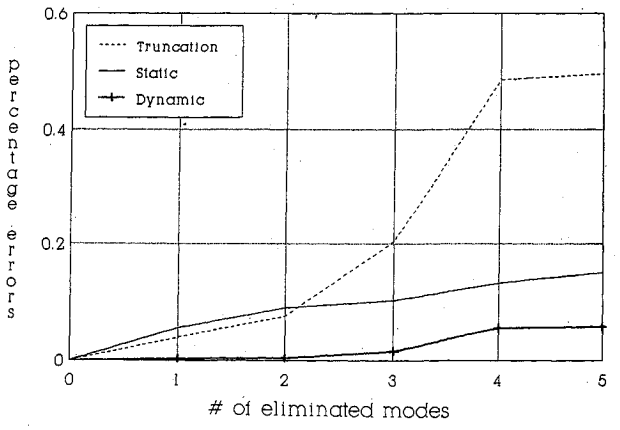

Fig. 8 Flutter frequncy errors, closed-loop, special constraints.

for given sets of structural, aerodynamic, and control parameters. A comparison of the MicroVax 3200 computer time for calculating one set of system roots with various full-size and reduced-order models with n states is given in Table 3. The calculations include the construction of the system matrices, extraction of all the eigenvalues, and writing them on an output file. The reduction is based on eliminating the five highest frequency vibration modes. Advantage is taken of the fact that the bottom partitions of the static residualization matrices [Eq. (20)] are zero, such that the computation time added by the dynamic residualization (relative to truncation) is about twice that of the static residualization.

It can be deduced from Table 3 that the computation time is approximately proportional to n^3, which is typical to many matrix operations, and that the time added by the dynamic residualization is small compared to the time savings in the eigenvalue extraction. As a thumb rule, one may assume that the application of dynamic residualization costs the same computation time as adding two states (one structural mode) to the truncated model or adding one state to the statically residualized model. The considerable gains in model accuracy imply that the dynamic residualization suggested in this paper is very cost effective.

Conclusions

Reduced-order, time-domain aeroservoelastic modeling has been formulated with three types of high-frequency mode-elimination techniques: mode truncation, static residualization, and the new dynamic residualization. These techniques are especially effective when applied in conjunction with the minimum-state aerodynamic approximation method, which yields a relatively low number of aerodynamic states. A realistic numerical example demonstrated that, when applied to all the modes with natural frequencies above the range of important aeroelastic activity, the static and dynamic residualization errors are about 60% and 30% of the mode truncation errors. An additional improvement of the dynamic residualization accuracy may be obtained by applicaton of special zero-coefficient constraints in the aerodynamic approximation. However, these constraints might adversely affect the aerodynamic approximation accuracy and by that offset the residualization accuracy gains. The computation time added by application of the dynamic residualization is very small relative to the time savings in subsequent analyses with the reduced-order model.

References

[1]Bisplinghoff, R. L., Ashley, H., and Halfman, R. L., *Aeroelasticity,* Addison-Wesley, MA, 1955.

[2]Bisplinghoff, R. L., and Ashley, H., *Principles of Aeroelasticity,* Wiley, New York, 1962.

[3]Albano, E., and Rodden, W. P., "A Doublet-Lattice Method for Calculating Lifting Disturbances of Oscillating Surfaces in Subsonic Flow," *AIAA Journal,* Vol. 7, No. 2, 1969, pp. 279–285.

[4]Adams, W. M., Jr., Tiffany, S. H., Newsom, J. R., and Peele, E. L., "STABCAR—A Program for Finding Characteristic Roots of Systems Having Transcendental Stability Matrices," NASA TP-2165, June 1984.

[5]Abel, I., Newsom, J. R., and Dunn, H. J., "Application of Two Synthesis Methods for Active Flutter Suppression on an Aeroelastic Wind-Tunnel Model," *Proceedings of the AIAA Atmospheric Flight Mechanics Conference of Future Space Systems,* AIAA, New York, Aug. 1979, pp. 93–103.

[6]Mukhopadhyay, V., Newsom, J. R., and Abel, I., "A Method for Obtaining Reduced-Order Control Laws for High-Order Systems Using Optimization Techniques," NASA TP-1876, Aug. 1981.

[7]Arbuckle, P. D., Buttrill, C. S., and Zeiler, T. A., "A New Simulation Model Building Process for Use in Dynamics Systems Integration Research," *Proceedings of the AIAA Flight Simulation Technologies Conference,* AIAA, New York, Aug. 1987.

[8]Karpel, M., "Sensitivity Derivatives of Flutter Characteristics and Stability Margins for Aeroservoelastic Design," *Journal of Aircraft,* Vol. 27, No. 4, 1990, pp. 368–375.

[9]Tiffany, S. H., and Adams, W. M., Jr., "Nonlinear Programming Extension to Rational Approximaton Methods of Unsteady Aerodynamic Forces," NASA TP-2776, July 1988.

[10]Peele, E. L., and Adams, W. M., Jr., "A Digital Program for Calculating the Interaction Between Flexible Structures, Unsteady Aerodynamics, and Active Controls," NASA TM-80040, Jan. 1979.

[11]Karpel, M., "Design for Active and Passive Flutter Suppression and Gust Alleviation," NASA CR-3482, Nov. 1981.

[12]Karpel, M., "Time-Domain Aeroservoelastic Modeling Using Weighted Unsteady Aerodynamic Forces," *Journal of Guidance, Control, and Dynamics,* Vol. 13, No. 1, 1990, pp. 30–37.

[13]Karpel, M., and Hoadley, S. T., "Physically Weighted Minimum-State Unsteady Aerodynamic Approximation," NASA TP (to be published).

[14]Nissim, E., and Lottati, I., "An Optimization Method for the Determination of the Important Flutter Modes," *Journal of Aircraft,* Vol. 18, No. 8, 1981, pp. 663–668.

[15]Sheena, Z., and Karpel, M., "Static Aeroelastic Analysis Using Aircraft Vibration Modes," *Collection of Papers of the Second International Symposium on Aeroelasticity and Structural Dynamics,* Aachen, FRG, April 1985, pp. 229–232.